IEEE Access
Multidisciplinary | Rapid Review | Open Access Journal

Received December 18, 2020, accepted December 30, 2020, date of publication January 8, 2021, date of current version January 19, 2021.

Digital Object Identifier 10.1109/ACCESS.2021.3050043

Beam Divergence Reduction of Vortex Waves With a Tailored Lens and a Tailored Reflector

MOHAMED HAJ HASSAN[1], BENEDIKT SIEVERT[1], (Member, IEEE), JAN TARO SVEJDA[1], (Member, IEEE), AYA MOSTAFA AHMED[2], JAN BAROWSKI[3], (Senior Member, IEEE), ANDREAS RENNINGS[1], (Member, IEEE), ILONA ROLFES[3], (Member, IEEE), AYDIN SEZGIN[2], (Senior Member, IEEE), AND DANIEL ERNI[1], (Member, IEEE)

[1]General and Theoretical Electrical Engineering (ATE), Faculty of Engineering, CENIDE–Center for Nanointegration Duisburg-Essen, University of Duisburg-Essen, 47048 Duisburg, Germany
[2]Department of Electrical Engineering, Ruhr-Universität Bochum, 44801 Bochum, Germany
[3]Institute of Microwave Systems, Ruhr-Universität Bochum, 44801 Bochum, Germany

Corresponding author: Mohamed Haj Hassan (mohamed.haj-hassan@uni-due.de)

This work was supported in part by the Deutsche Forschungsgemeinschaft (DFG, German Research Foundation)—TRR 196 MARIE in the framework of projects S03, C05, and M02, under Grant 287022738, and in part by the University of Duisburg-Essen through the Open Access Publication Fund.

ABSTRACT Reducing the strong beam divergence inherent to Orbital Angular Momentum waves (also known as OAM waves or vortex waves), a tailored lens and a tailored reflector are presented in this study. The generation of the OAM waves is accomplished by a Uniform Circular Patch Antenna Array (UCA) operating at 10 GHz. Here, the tailored lens and reflector are set up by two correspondingly designed shape functions rotated around the antenna's center axis in broadside direction (i.e. body of revolution approach). Initially, the tailored lens is introduced to be compared to the UCA in the presence and absence of the conventional lens separately. Upon the usage of the tailored lens, a gain improvement of 5.8 dB has been obtained in the simulation compared to a gain of 4.8 dB in the measurement. On the other hand, the tailored reflector is set under the same procedure to be compared also to the UCA with and without a conventional reflector. Both of the reflectors are simulated under idealized conditions with the aid of an OAM impressed field source used as an emitter for a meaningful comparison. The simulated gain has shown a better performance accomplished by the tailored reflector as the height r_0 reaches a level less than $1.5\,\lambda$ as well as the opening angle ϑ is less than $38\,^\circ$ (given an UCA with an element separation distance $d = \lambda/2$). Furthermore, three different ground plane shapes with realistic UCA are applied for the simulation procedure where each of them is perturbing the radiation of the reflector. All of the lenses and the reflectors are manufactured and later measured in an anechoic chamber to undergo a comparison with the simulated results. This article demonstrates that the vortex waves need a tailored lens or a tailored reflector to decrease the beam divergence effectively especially when the radius of the UCA becomes increasingly large.

INDEX TERMS Vortex waves, orbital angular momentum OAM, spiral waves, patch antenna array, reflector, lens.

I. INTRODUCTION

In recent years, vortex waves have attracted the interest of many scientists, especially after the successful utilization of vortex waves in the field of optics [1]. Electromagnetic waves can carry Spin Angular Momentum (SAM) (intrinsic rotation, corresponding to circularly polarized waves) and Orbital Angular Momentum (OAM) (extrinsic rotation having a macroscopic helical phase front) [2]. The vortex waves are characterized firstly by a helical phase distribution that changes linearly around the beam axis, and secondly by a doughnut-shaped radiation pattern, where the phase in the center, namely on the beam axis, is not determinable defining thus a phase singularity. The vortex waves are described with

The associate editor coordinating the review of this manuscript and approving it for publication was Weiren Zhu.

the following relation $\boldsymbol{E}(\rho, \varphi) = E_0(\rho)\exp(j\varphi m)\boldsymbol{e}_r$, where $E_0(\rho)$ is the amplitude of the electric field strength, φ is the geometric azimuthal angle and m is the OAM mode order. There are many options to generate OAM waves such as elliptical patch antennas (supporting two simultaneously excited orthogonally oriented resonant modes) [3], [4], uniform circular patch antenna arrays (UCA) [5], spiral phase plates [6], holographic plates [7], metasurfaces [8], and reflectors [9]. Each of these approaches have its advantages and disadvantages, regarding e.g. costs, fabrication simplicity, integration capability, simple design and implementation, simple feeding etc. The vortex waves contain unlimited number of mutually orthogonal mode orders $m \in \{\ldots, -2, -1, 0, 1, 2, \ldots\}$ creating an additional degree of freedom in signal coding not to mention a new spatial division multiplexing (SDM). This yields an independent data stream at the same operating frequency, thus an improvement in the capacity as well as in the spectral efficiency. Moreover, a new physical transmission technique is earned by the OAM mode division multiplexing (OAM-MDM) which can be also combined to other types of multiplexing (time, polarization, frequency, and code). Such combination can lead to a large enhancement in the data transmission [10]. Additionally, the OAM waves are beneficial through increasing the digit value in the RFID technology with the aid of helically arranged dielectric resonator array instead of just one dielectric resonator. Otherwise, the conventional 0 and 1 digits are provided by the dielectric resonator [11]. In addition, it is also capable of rejecting the clutter coming from the broadside direction [12]. Furthermore, the vortex waves are beneficial for the imaging of the fixed objects and can provide extra features for target localization where the Doppler effect is less complicated than the conventional radar application [13]. Nevertheless, the vortex waves are suffering from the strong beam divergence, especially when higher OAM mode orders are needed [14]. This beam divergence can be an issue for many applications, like in the wireless communication and in particular when using OAM beams in material characterization within advanced reflectometry schemes. As noticed, this beam divergence reduction is not performed to be used in the MIMO application. Several publications have documented considerable efforts to reduce the beam divergence by using Fabry-Perot Cavity [15], lenses, [16]–[19], antenna arrays in UCA [20], and reflectors [9], [21]–[24]. Here, our choice fell on the uniform circular patch antenna array (UCA) approach to be designed with a tailored lens and a tailored reflector to reduce the OAM beam divergence. These two approaches can also be compared to the ones of metasurfaces [8] and multi UCAs [25], where both methods support large effective apertures and thus reduced beam divergences. The simulated and measured gain of the two approaches are compared to those of the UCA, and to the conventional lens and conventional reflector. The initial idea has been presented in an earlier paper, where a tailored lens is only simulated and compared to cases including and excluding the conventional one [26]. In the following, the proceeding Section II discusses the impact of the distance d between the adjacent antenna elements on the radiation pattern. Whereas, the following Sections III and IV present the simulated and the measured phase front, near- and far-field of the conventional and tailored lenses. Then, the same procedure is carried out for the reflector with an OAM impressed source and with realistic UCA in Sections V and VI. After that, Section VII introduces the measured gain and phase front of the reflector. Finally, Section VIII concludes the findings of this article.

II. DESIGN OF UNIFORM CIRCULAR ARRAY (UCA)

In the setup, a single rectangular patch antenna element of 7.4 mm length (about $\lambda_{\text{eff}}/2$) and 10.8 mm width is designed on a 30 mm × 30 mm printed circuit board (PCB). Two insets in the antenna enable the matching of the antenna to 50 Ω so that the realized gain is maximized to 7 dBi. The antenna is linearly polarized in the y-direction (according to the coordinate system given in Fig. 1 (a). In the following, this single antenna is extended to form a circular patch antenna array of 8 elements with a distance between the adjacent antennas of $d = \lambda/2$ (cf. Fig. 1 (b)) in order to obtain the desired optimized OAM waves characterized by a doughnut type radiation pattern, increased gain and lower side and back lobes. However, the slight asymmetry of the radiation pattern (cf. Fig. 1 (b)) is due to the single-sided, hence asymmetric feeding of each patch antenna element. As a result, this asymmetry is more noticeable for larger radii. The following equations are representing the analytical expressions for the electric field of the vortex waves in cylindrical coordinate system $\boldsymbol{E}(\rho, \varphi, z)$ propagating along the z-direction

$$E_\rho = j\frac{Z_0\omega m}{k\rho}E_0J_l(k_\rho\rho)e^{-jk_zz}e^{-jm\varphi}, \tag{1}$$

$$E_\varphi = -\frac{Z_0\omega k_\rho}{k}E_0J_l'(k_\rho\rho)e^{-jk_zz}e^{-jm\varphi}, \tag{2}$$

$$E_z = 0, \tag{3}$$

where Z_0 is the free-space wave impedance, ω is the angular frequency, m is the OAM mode order, E_0 is the wave amplitude, $J_l(k_\rho\rho)$ is the l^{th} order Bessel function, k_0 is the free-space wave number

$$k_0^2 = k_\rho^2 + k_z^2 = \frac{\omega^2}{c^2}, \tag{4}$$

where c is the speed of light [27]. As noted, due to the practical focus of the article, there is no need to discuss too much the theoretical part of the electric and magnetic field of the OAM waves. Furthermore, this study aims to reduce the beam divergence in the broadside direction, i.e. the radiated direction, where the gain of the main lobe would be increased. Moving on, the reflection coefficient S_{11} of the antennas is between −17 dB and −20 dB at the operating frequency of 10 GHz, and the gain of the planar circular patch antenna array amounts to about 9.5 dBi for the OAM mode order $m = -1$. Moreover, the footprint of the underlying PCB board is 100 mm × 100 mm. The UCA is designed with the

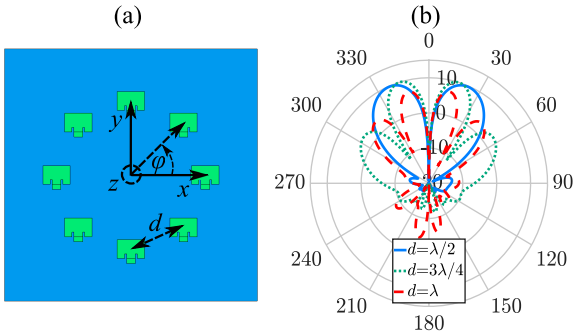

FIGURE 1. Top view of the UCA (a), the simulated radiation pattern (dBi) of the UCA for the OAM mode order −1 at $\varphi = 0°$ (*H*-plane) for an element separation d of $\lambda/2$, $3\lambda/4$, and λ ($\lambda = 30$ mm at 10 GHz) (b).

full-wave computational electromagnetics simulator FEKO that processes the Method of Moments (MoM) generating a high simulation efficiency for this setup. For a better manageability, the operating frequency is set to 10 GHz. These antennas are patterned on a Rogers RO4003C substrate with a height of 1.524 mm and a relative permittivity of 3.55. The phase shift between each pair of adjacent antennas is defined by the port feeding phase in the full-wave simulator FEKO to obtain the OAM mode with mode order $m = -1$. Thus, it is defined by the following relation

$$\varphi_1 = \frac{2\pi m}{N}, \tag{5}$$

where N denotes the number of single antenna and m is the mode order of the vortex waves.

III. DESIGN OF CONVENTIONAL AND TAILORED LENS

In this section, the conventional lens and the tailored lens are set up for comparison. Both of the two lenses are made of polypropylene with a 2.2 relative permittivity. However, the dielectric loading is causing an alteration in the effective permittivity, thus the antennas need to be redesigned accordingly. The new length and width of the patch antenna element are 7.25 mm and 10.2 mm, respectively. Moreover, the reflection coefficient S_{11} amounts to −37.6 dB for one patch antenna element at 10 GHz. As displayed in Fig. 2 (a), the conventional lens is divided into two parts, namely the cylindrical dielectric part and the ellipsoidal part. The cylindrical dielectric part shifts the focal point into the center of the UCA, while the ellipsoidal part converts the divergent spherical waves into a narrower beam. Therefore, the gain of the UCA is expected to increase, whereas the divergence would correspondingly decrease. The design of the conventional lens uses the following equations [28] according to Fig. 2 (a, c, and e)

$$b = \frac{a}{\sqrt{1 - \frac{1}{\Re(\varepsilon_r)}}}, \tag{6}$$

$$L = \frac{b}{\sqrt{\Re(\varepsilon_r)}}, \tag{7}$$

$$D[\text{dB}] = 20\log_{10}\left(\frac{2\pi a}{\lambda}\right), \tag{8}$$

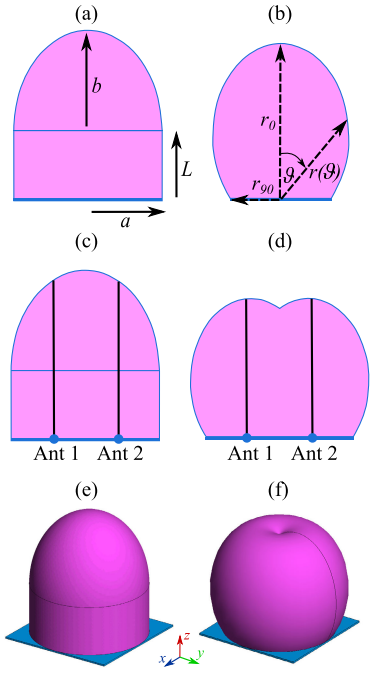

FIGURE 2. Conventional lens (a, c, and e), and tailored lens (b, d, and f).

where a is the semi-minor axis of the ellipsoidal part along the z-axis, which depends on the target directivity in [dB], and b is the semi-major axis. L is signified as the length of the extension part, and λ is the operating wavelength which happens to be 30 mm at 10 GHz. But, the equation (8) seems to assume an aperture efficiency of 100% which is most probably false in the context of the presented OAM antennas. a is chosen to be 50 mm so that the assembly and the centering of the lens on the PCB board are simplified, whereas the radius of the UCA is 19.6 mm. Hence, L is 45.6 mm, and b is 67.7 mm. On the other hand, the principle of Fermat permits to design a lens for a single patch antenna [29]

$$r(\vartheta) = \left(\frac{r_0(n_1 - n_0)}{n_1 - n_0\cos(\vartheta)}\right), \tag{9}$$

where n_1 is the refractive index of the lens with the value of 1.483, and n_0 is the refractive index of the air with values of 1. The radius of the lens $r(\vartheta)$ relies on the polar angle ϑ, so r_0 is the radius at the polar angle $\vartheta = 0°$. The shape function (9) designs the tailored lens by means of sweeping this function which is shifted to align with the patch antenna's center around the z-axis, as shown in Fig. 2 (b, d, and f). Similar to the conventional lens, the entire PCB board is covered to simplify the assembling of the lens with the UCA. Thus, the radius at the polar angle $\vartheta = 0°$ and $\vartheta = 90°$ are about 93 mm and 30.4 mm, respectively. As r_0 gets larger, the gain of the antenna increases inversely to the divergence which is correspondingly reduced. The gain of the UCA for the OAM mode order −1 with the conventional lens increases from about 9.5 dBi to 11.3 dBi as depicted in Fig. 3 (b). Similarly, the number of the side lobes increases leading automatically

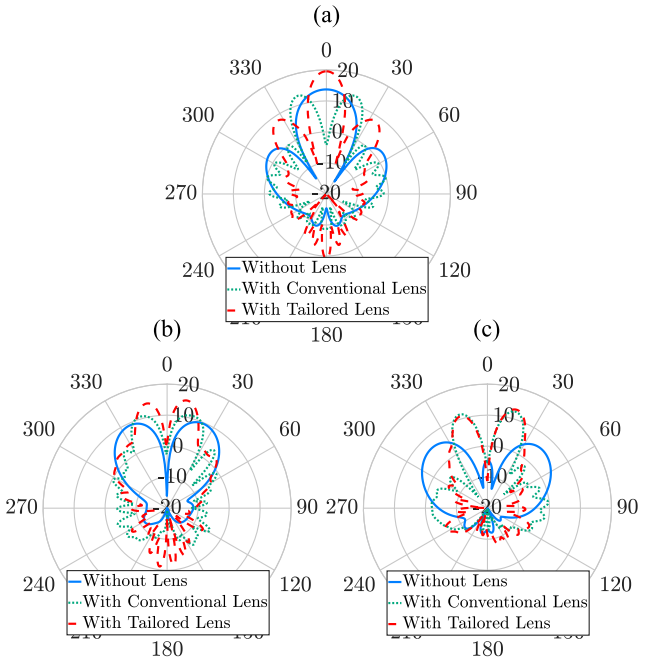

FIGURE 3. The simulated radiation pattern (dBi) of UCA at $\varphi = 0°$ (*H*-plane) for the cases of without lens, with conventional lens and with tailored lens for the OAM mode order 0 (a), −1 (b), and −2 (c).

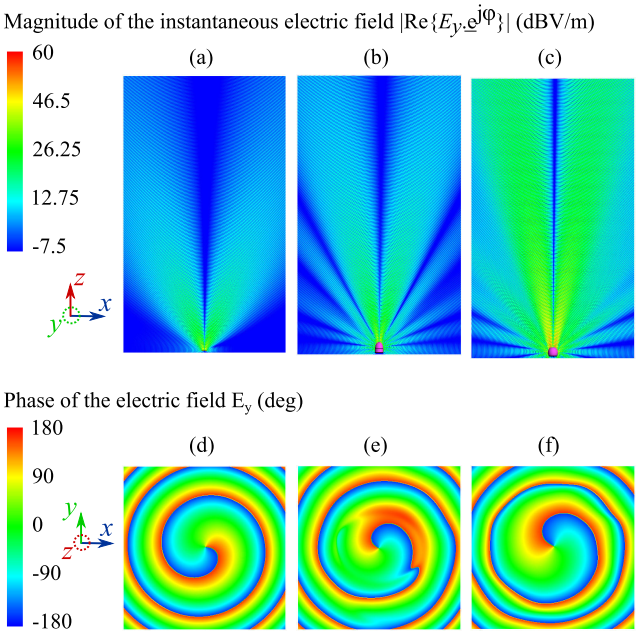

FIGURE 4. The simulated magnitude of the instantaneous electric field and the simulated phase distribution for the OAM mode order −1 of the cases without lens (a, and d), with conventional lens (b, and e), and with tailored lens (c, and f), respectively.

to the decline of the gain and the beam divergence. In contrast, the tailored lens (cf. Fig. 3 (b)) presents a significant decrease in the beam divergence with a maximum gain showing a 15.3 dBi value. Moreover, the number of side lobes is lower than the one in case of the conventional lens. The apertures of the two lenses are different, where the effective aperture A_e, and the physical aperture A_{phys} are defined with [30]

$$A_e = \frac{\lambda^2 G}{4\pi}, \tag{10}$$

$$A_{phys} = \pi r_{max}^2, \tag{11}$$

$$e_a = \frac{A_e}{A_{phys}}, \tag{12}$$

where λ is the wavelength in free space, and G signifies the gain of the antenna. r_{max} is represented by a concerning the conventional lens, while it is considered the maximum of $r(\vartheta)\sin(\vartheta)$ for the case of tailored lens (cf. Fig 2 (a, and b). The ratio between the effective aperture and the physical one determines how effective an antenna can be upon receiving electromagnetic waves. This ratio is called the aperture efficiency e_a covering a range between 0 and 1. Considering the conventional lens, its aperture efficiency is 0.12 unlike the tailored lens which has 0.21 value. Thus, the tailored lens tends to be superior over the conventional. In Fig. 3 (a), the mode order 0 is depicted, but it is deformed by the conventional lens, while the tailored lens enhances the gain from 13.7 dBi to 19.5 dBi. This beam deformation of the zeroth mode with the conventional lens occurs because of the displacement of the antennas from the focal point of the lens yielding a refraction of the waves in an undesirable direction. By increasing the aperture of the lens, the displacement error decreases, and the issue would be minimized. This abnormal behavior of the conventional lens with the zeroth order mode gives preference to the tailored lens over the conventional one especially when used in the OAM target localization where several OAM mode orders are necessary to localize the target. In Fig. 3 (c), once mode −2 is set, the two lenses yield similar gain enhancements but with higher side lobe suppression levels with the tailored lens. Note that the maximum gain with the second mode order can be achieved with a distance d of about λ between the adjacent antenna element (cf. Fig. 1 (a)). Therefore, the size difference between the conventional and the tailored lens will be very large giving additional benefit for the tailored lens. Fig. 4 introduces the instantaneous electric field and the phase distribution of the OAM mode order −1 of the cases without lens (a, and d), with conventional lens (b, and e) and with tailored lens (c, and f).

IV. LENS FABRICATION AND MEASUREMENTS

The designed conventional and tailored lens in the previous section have been manufactured by an external company with the help of a 3D printing machine. The measurement is performed by a vector network analyzer (VNA) ZVA 40 from Rohde & Schwarz in an anechoic chamber hence avoiding unwanted reflections and distortions. A standard gain horn antenna is utilized as a transmitter, whereas the assembled lens with the UCA and the Butler matrix (BM) are used as a receiver. The BM is the one responsible for generating the different OAM mode orders. The distance separating the transmitter and the receiver is about 5 m where the lens,

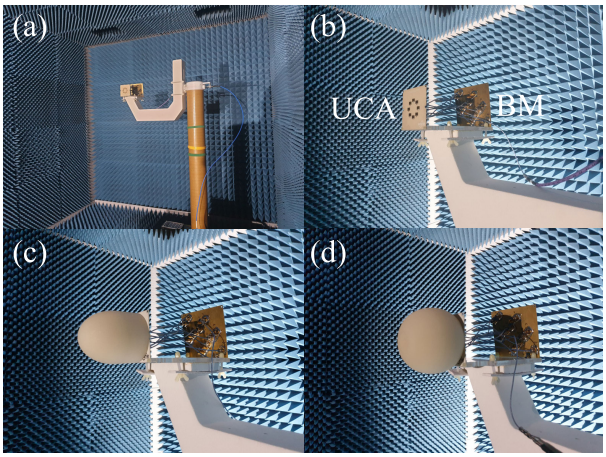

FIGURE 5. The rotary table in the anechoic chamber (a), the manufactured UCA with Butler matrix (BM) (b), the conventional lens on the UCA (c), and the tailored lens on the UCA (d).

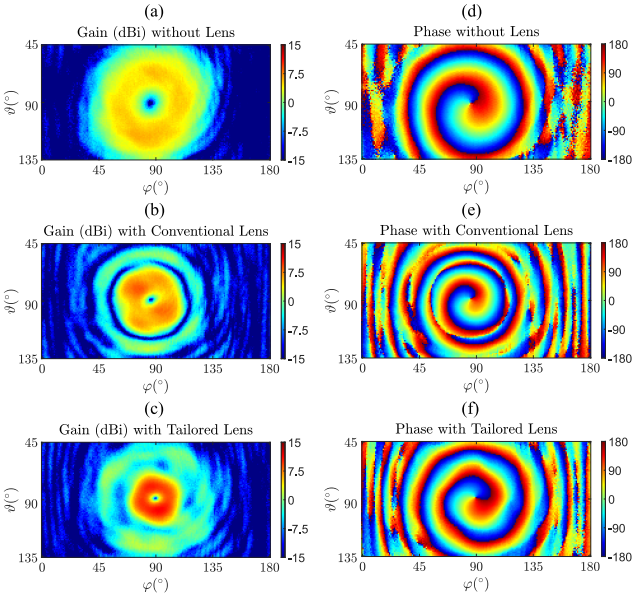

FIGURE 6. The measured gain (dBi) and the measured phase distribution for the OAM mode order 1 of UCA without lens (a, and d), with conventional lens (b, and e), and with tailored lens (c, and f).

accompanied by the UCA and the BM, are mounted on a rotary table rotating in the azimuth angle φ from 0° to 180° and in the elevation angle ϑ from 45° till 135°. The OAM mode order 1 is provided by the 8 × 8 BM which is connected to the UCA by eight coaxial cables of equal length of 200 mm (cf. Fig. 5). Furthermore, the two lenses are assembled separately on the UCA (cf. Fig. 5 (c, and d)) to be validated. Fig. 6 (a, b, and c) demonstrate the gain without lens, with conventional lens and with tailored lens, respectively. Compared to the others, the tailored lens achieved a further superior performance by reducing the beam divergence more. In addition, the gain is increased by 1.7 dBi to reach 9.7 dBi level regarding the conventional lens and by 4.8 dBi reaching 12.8 dBi in case of the tailored lens.

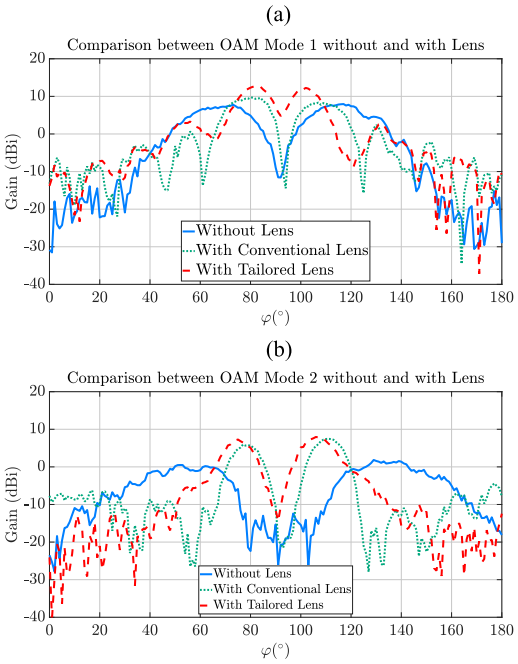

FIGURE 7. Comparison between the measured gain (dBi) of the UCA at $\vartheta = 0°$ (H-plane) without lens, with conventional lens, and with tailored lens for the OAM mode order 1 (a), and 2 (b).

Meanwhile, in Fig. 6 (d, e, and f) the radiation possesses a helical phase distribution of one helix according to the first OAM mode order. An OAM mode of order m is characterized by m number of helices in the phase front with a phase distribution of $\alpha(\varphi) = m\varphi$ noting that φ ranges between 0 and 2π. Determining the positive OAM mode orders is done by the right-handed thread with respect to the propagation direction in which the vortex waves undergo clockwise rotation in contrast to the negative modes rotating in a counter-clockwise direction. Fig. 7 shows the measured gain in 2D (H-plane) of the three cases for the OAM mode order 1 (a) and 2 (b). Unlike the ideal case, it is noticeable that the gain in the center of the radiation pattern is not 0 (linear). This occurs due to several reasons such as the reflections in the BM and the misalignment between the transmitter and the receiver. And with more observation, higher divergence is seen when the OAM mode orders are raised.

V. DESIGN OF CONVENTIONAL AND TAILORED REFLECTOR WITH OAM IMPRESSED FIELD SOURCE

Likewise the lens, Fermat's principle enables a conventional reflector to be designed for a point source [29] characterized by $r(\vartheta)$ as a function of r_0 and n_1. $r(\vartheta)$ denotes the radius of the reflector hanging on the polar angle ϑ. On the second hand, r_0 is the radius at $\vartheta = 0°$, whereas n_1 is the refractive index of the air with a value of 1.

$$r(\vartheta) = \left(\frac{2r_0}{n_1(1+\cos(\vartheta))}\right). \tag{13}$$

The tailored reflector is achieved by sweeping the shape function which has been shifted to align the patch antenna's

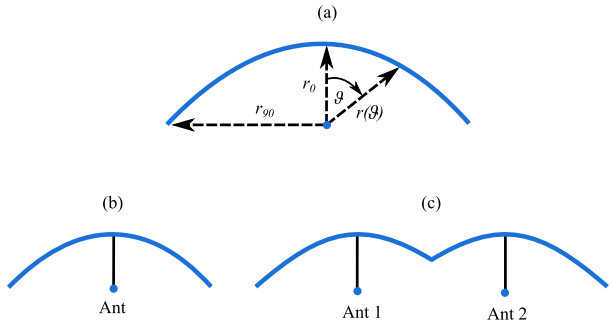

FIGURE 8. Reflector for a point source (a), extension to conventional reflector (b), and extension to tailored reflector (c).

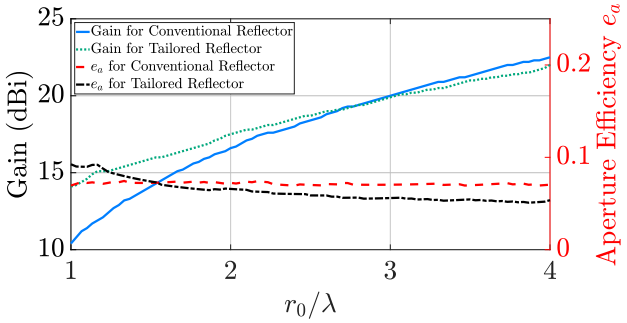

FIGURE 9. The simulated gain (dBi) for the OAM mode order −1 depending on the height r_0 of the reflector.

TABLE 1. The opening angle for the maximum simulated gain of each reflectors ($\lambda = 30$ mm at 10 GHz) for the OAM mode order −1.

r_0 (mm)	Opening angle (°) (Conventional reflector)	Opening angle (°) (Tailored reflector)
30	155	168
32	156	169
34	157	170
42	161	171
50	164	172
59	166	173
72	169	174
100	172	175
113	173	176

center around the z-axis (13), as shown in Fig. 8 (a, b, and c). The two reflectors depend on two parameters, namely the radius r and the angle ϑ. To be more specific, as the r and ϑ get higher, the gain increases. Consequently, the divergence of the vortex beams decreases due to the increased focusing of the radiation pattern. And, the angle ϑ is adjusted from $-90°$ till $90°$. The tailored reflector will be compared to the UCA with conventional reflector and to another one without any reflector. The gain of the two reflectors is presented in Fig. 9 revealing that superior performance is achieved by the tailored reflector compared to the conventional reflector especially with the height of 1.5λ. Despite that there is no big gain difference between the two reflectors beyond 1.5λ, the tailored reflector continues to administrate a higher reduction in the divergence because the maximum gain is even closer to the broadside radiation (cf. table 1). Note that these gain

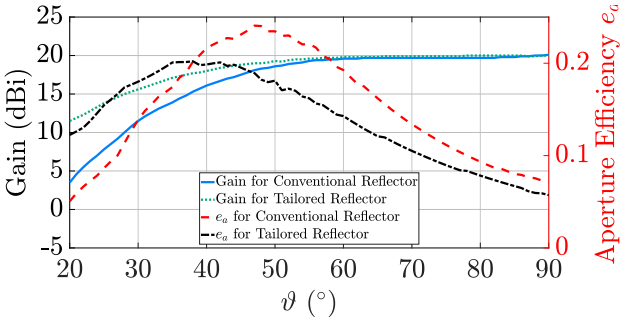

FIGURE 10. The simulated gain (dBi) for the OAM mode order −1 depending on the angle ϑ with a height r_0 of 90 mm using an OAM impressed field source with conventional reflector and with tailored reflector, and the aperture efficiency e_a of the two reflectors.

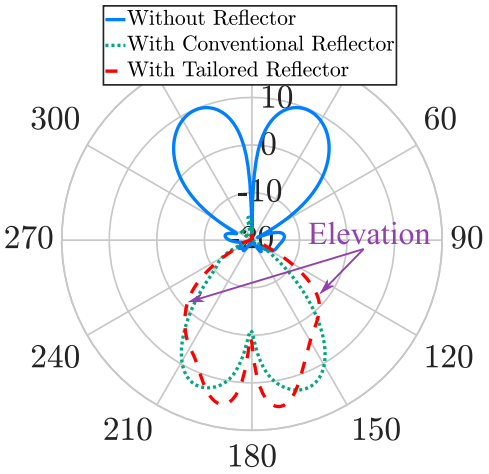

FIGURE 11. The simulated radiation pattern (dBi) using an OAM impressed field source for the OAM mode order −1 with r_0 of 40 mm and with an angle ϑ from −90° till 90° without reflector, with conventional reflector and with tailored reflector.

results are obtained without the impact of the ground plane which may cause some reflections and diffractions of the reflector radiation thus causing slight deviations in the comparison between the two reflectors. In Fig. 10, the comparison between the two reflectors is undergone as a function of angle ϑ in which the tailored reflector shows better accomplishment until the angle reaches $\vartheta = 38°$. In Fig. 11, the simulated radiation pattern using an OAM impressed field source at $\varphi = 0°$ (H-plane) without reflector, with conventional reflector and with tailored reflector are depicted seperately under 40 mm height and −90° till 90° ranged angle ϑ. The two reflectors reduce the divergence from about 9.5 dBi at angle 336° to 13.2 dBi at angle 160° (conventional) and to 15.4 dBi at angle 170° (tailored). Unfortunately, the tailored reflector causes a certain elevation of pattern due to the cut of the reflector in the middle allowing some rays to propagate into the second part of the reflector whereby undesired reflections can occur (cf. Fig 11). Whenever the UCA radius is larger or the height r_0 is lower, a decline of the elevation will occur. In Figs. 12 and 13, the instantaneous electric field and the helical phase front of the three cases are depicted. Generally,

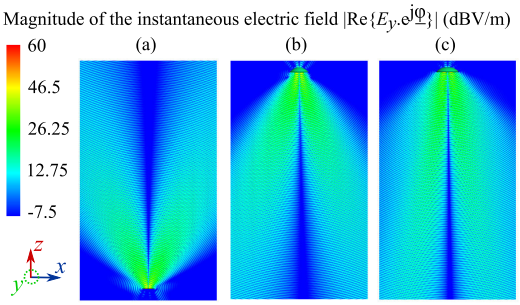

FIGURE 12. The simulated magnitude of the instantaneous electric field using an OAM impressed field source for the OAM mode order −1 with r_0 of 40 mm and with an angle ϑ from −90° till 90° without reflector (a), with conventional reflector (b) and with tailored reflector (c).

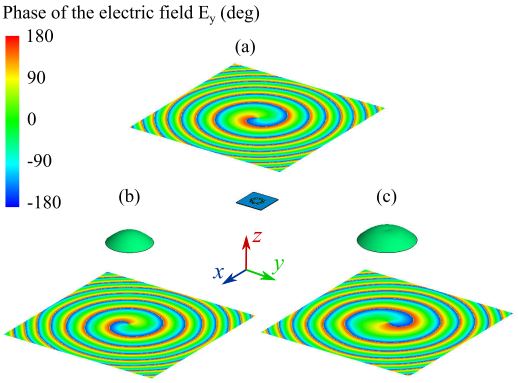

FIGURE 13. The simulated phase distribution of E_y using an OAM impressed field source for the OAM mode order −1 (from $x = -300$ till 300 mm, from $y = -300$ till 300 mm, $z = 300$ mm for (a) and $z = -300$ mm for (b, and c)) indicating the phase distribution of OAM impressed field source with r_0 of 40 mm and with an angle ϑ from −90° till 90° without reflector (a), with conventional reflector (b) and with tailored reflector (c).

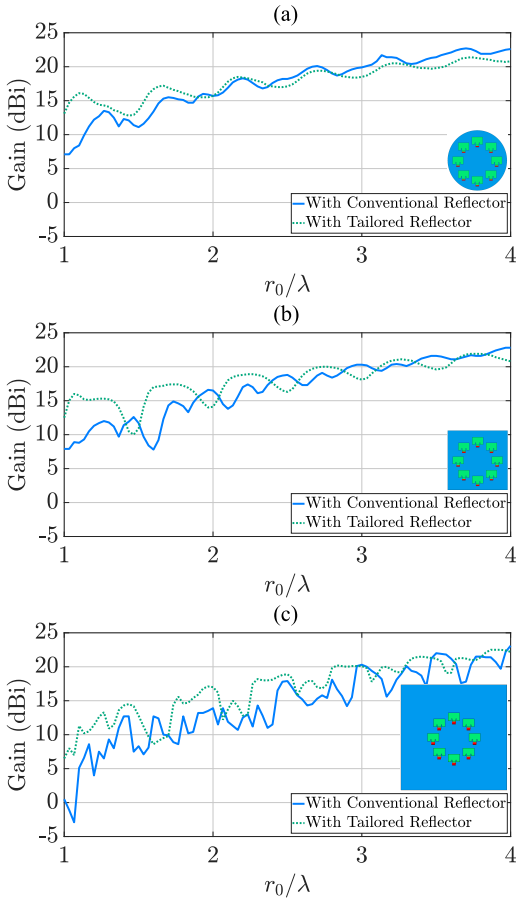

FIGURE 14. The simulated gain (dBi) of the realistic UCA for the OAM mode order −1 depending on the height r_0 of the reflector with a 60 mm diameter circular ground plane (a), for a 60 mm × 60 mm rectangular ground plane (b) and for a 100 mm × 100 mm rectangular ground plane (c).

the OAM mode order is inverted after the reflection with the reflectors, namely +1 instead of −1.

VI. REFLECTOR EVALUATION INCLUDING REALISTIC FEEDING ANTENNA STRUCTURE

In the prior section, the three cases are presented using an OAM impressed field source to simplify the interpretation of the reflector's behavior. While in this section, the reflectors are simulated with a realistic UCA mounted on three different shaped ground planes. The first shape is a circular PCB with a diameter of 60 mm, whereas the second and the third shapes consists of a rectangular PCB with a footprint of 60 mm × 60 mm and 100 mm × 100 mm, respectively. Fig. 14 establishes the gain according to the height r_0 in an angle ϑ ranging from −90° till 90° in which the gain oscillation is caused by the ground plane due to the standing waves between the UCA and the reflector. The three different shaped ground planes manipulate the gain of the conventional reflector more than the tailored one. In Fig. 15, the gain based on the angle ϑ with a height r_0 of 90 mm is depicted. The circular ground plane shape has minimal effect on the gain of the reflectors giving it the priority for the reflectors. Figs. 16 and 17 display the radiation pattern for the OAM mode order −1 of the two reflectors in 2D at $\varphi = 0°$ (H-plane) for heights r_0 of 30 mm, 51 mm, and 120 mm. As shown, the tailored reflector performs well with the height r_0 of λ unlike the conventional reflector which reveals a distinctly shaped OAM beam with the height r_0 of 1.67λ. In Figs. 18 and 19, the instantaneous electric field and the phase distribution of the (60 mm × 60 mm) rectangular shaped UCA for the OAM mode order −1 with 40 mm height r_0 and with an angle ϑ from −90° till 90° are introduced. The helicity of the front phase is still maintained but with opposite OAM mode order's sign, namely from the mode −1 to the mode 1, and with higher distortion for the conventional reflector. Fig. 20 shows the radiation pattern of the OAM mode orders 0, −1 and −2 with a height of 90 mm and an angle ϑ of 45°. In the case of the zeroth mode order, the tailored reflector increases the gain from 13.9 dBi to 19.6 dBi in contrast to the conventional reflector that decreases the gain till 10.3 dBi. This is noted as a similar behavior to that of the conventional lens compared to the tailored lens. With respect to the first OAM mode order, the gain of the conventional and tailored reflector is increased from about 9.5 dBi till

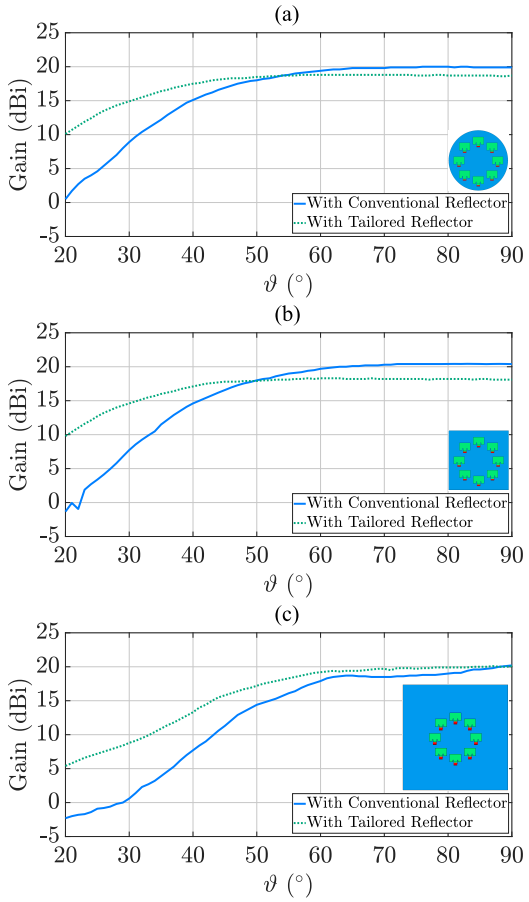

FIGURE 15. The simulated gain (dBi) of the realistic UCA for the OAM mode order −1 depending on the angle ϑ of the reflector for the mode order −1 with a height r_0 of 90 mm with a 60 mm diameter circular ground plane (a), for a 60 mm × 60 mm rectangular ground plane (b) and for a 100 mm × 100 mm rectangular ground plane (c).

16.5 dBi and 17.8 dBi, respectively. The tailored reflector yields 1.3 dBi more than the conventional reflector. While for the second OAM mode order, the gain of the conventional and the tailored reflector is increased from 6.3 dBi till 10.4 dBi and 13.9 dBi, respectively. Once the mode orders increase, the gain decreases because of the raised divergence. Similar to the tailored lens, the tailored reflector offers a benefit of saving material consumption especially for larger UCA radii in addition to extra antenna elements. Noting that the production and the equipment are limited, a reflector with a height of 90 mm and an angle of 45° is chosen.

VII. REFLECTOR FABRICATION AND MEASUREMENTS

In the same manner as the lens, a conventional reflector and a tailored reflector with a height of 90 mm and an opening angle ϑ of 45° are manufactured using a 3D printing machine to be measured in the anechoic chamber over a rotating stage. The reflectors consist of polypropylene which should be covered with aluminium foil in order to behave like a reflector. The reflector is assembled with the UCA and with the BM as shown in (cf. Fig 21). In Fig. 22, the beam

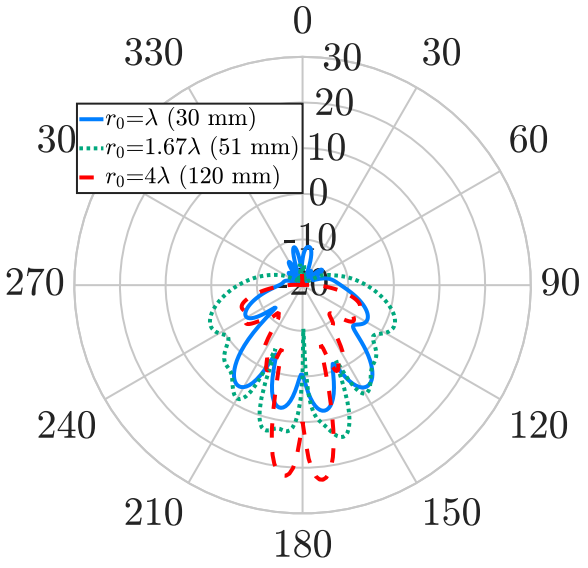

FIGURE 16. The simulated radiation pattern (dBi) with realistic UCA for the OAM mode order −1 of conventional reflector of UCA with a rectangular shaped PCB 60 mm × 60 mm for several height r_0 of 30 mm, 51 mm, and 120 mm.

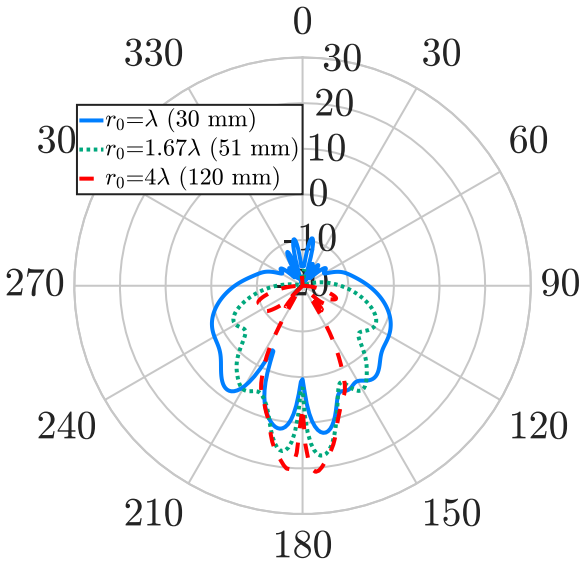

FIGURE 17. The simulated radiation pattern (dBi) with realistic UCA for the OAM mode order −1 of tailored reflector of UCA with a rectangular shaped form 60 mm × 60 mm for several height r_0 of 30 mm, 51 mm, and 120 mm.

divergence of the OAM mode order 1 is obviously reduced. The tailored reflector submits values of 12 dB as measured and 17.8 dB as simulated. Whereas 10.5 dB measured gain and 16.5 dB simulated one are revealed with the conventional one (cf. Fig. 23 (a)). As noticed, there is a variation between the measured and simulated values. This is due to the proceeding mentioned issues. First of all, the reflectors are not completely smooth due to the 3D printing method. On the second hand, the aluminium layers are not perfectly bonded to the UCA, and the antennas are fixed with a plastic patch that creates a certain absorption and delay of the reflected vortex

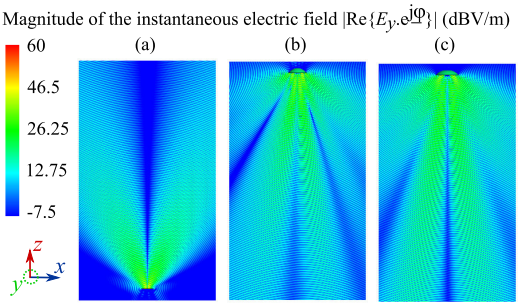

FIGURE 18. The simulated magnitude of the instantaneous electric field with a realistic UCA for the OAM mode order −1 of the circular antenna array with rectangular shaped PCB 60 mm × 60 mm without reflector (a), with conventional reflector (b), and with tailored reflector (c).

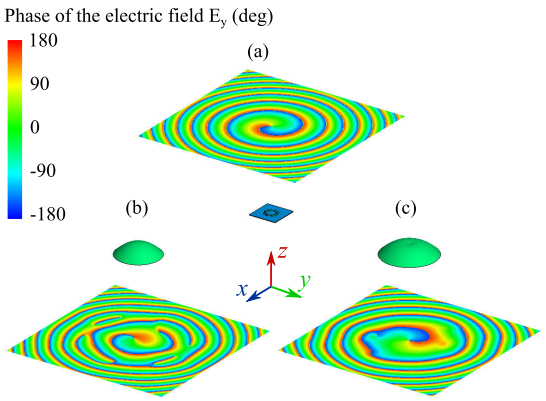

FIGURE 19. The simulated phase distribution of E_y with a realistic UCA for the OAM mode order −1 with rectangular shaped PCB 60 mm × 60 mm (from $x = -300$ till 300 mm, from $y = -300$ till 300 mm, $z = 300$ mm for (a) and $z = -300$ mm for (b, and c)) indicating the helical phase distribution of circular antenna array without and with reflector.

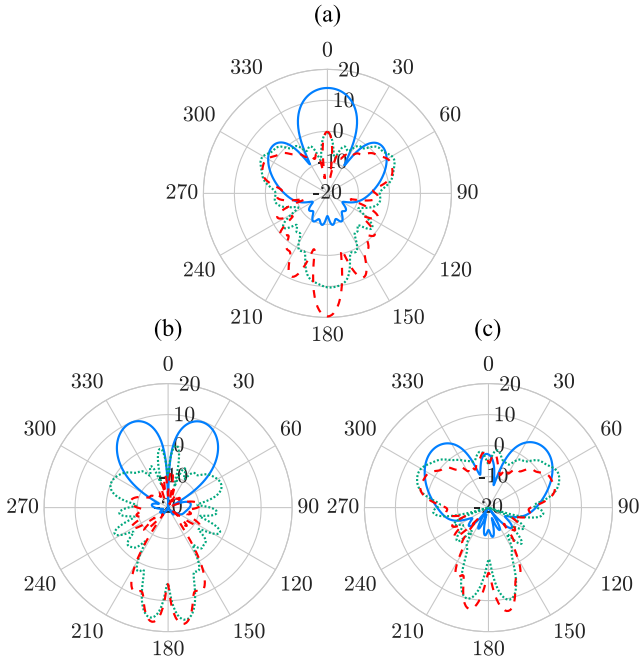

FIGURE 20. The simulated radiation pattern (dBi) with a realistic UCA for the three cases for the OAM mode order 0 (a), −1 (b), and −2 (c) at $\varphi = 0°$ (H-plane) with a height of 90 mm and an angle of 45°.

waves. Therefore, the UCA and the reflector are not perfectly in alignment. Furthermore, the antennas are supplied with

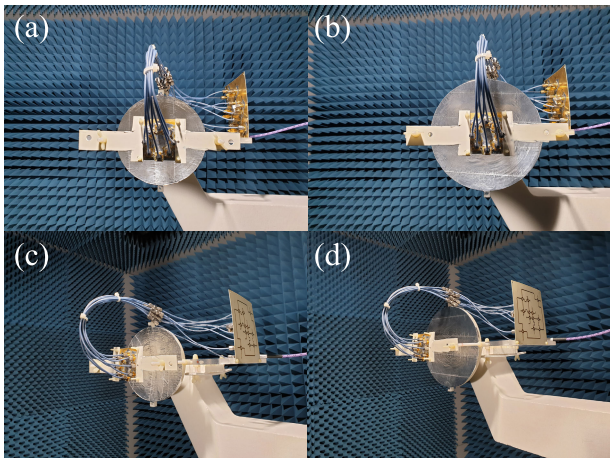

FIGURE 21. The manufactured conventional reflector (a, and c), and tailored reflector (b, and d).

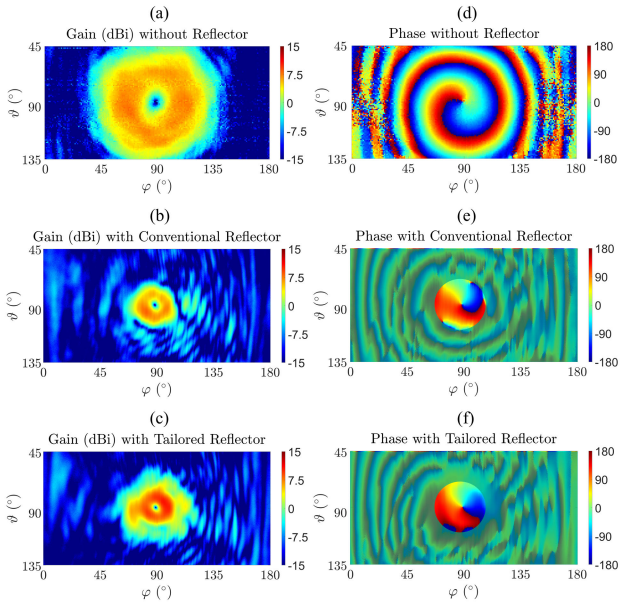

FIGURE 22. The measured gain (dBi) and the measured phase distribution of antennas for the OAM mode order 1 without reflector (a, and d), with conventional reflector (b, and e), and with tailored reflector (c, and f) with rectangular ground plane shape 60 mm × 60 mm (height of 90 mm and angle of 45°).

eight coaxial cables which can interfere with the path of the vortex waves. Nonetheless, in order to avoid such issues, the BM or the power divider (PD) [31] can be integrated into the ground plane, otherwise two reflectors (primary and secondary) such as the Cassegrain reflector can be applied. The phase distribution of the three cases which displays a distinct helical phase distribution of the first OAM mode order are also presented in the figure 22. Note that aiming for the helical phase distribution in the doughnut radiation pattern is purposed. Fig. 23 shows the gain for the OAM mode order 1 and 2 at $\varphi = 0°$ (H-plane). The measured gain of OAM mode order 2 (7.7 dBi) administers a gain enhancement of 4.5 dB and 3.1 dB compared to the UCA without reflector and with conventional reflector, respectively (cf. Fig. 23 (b)).

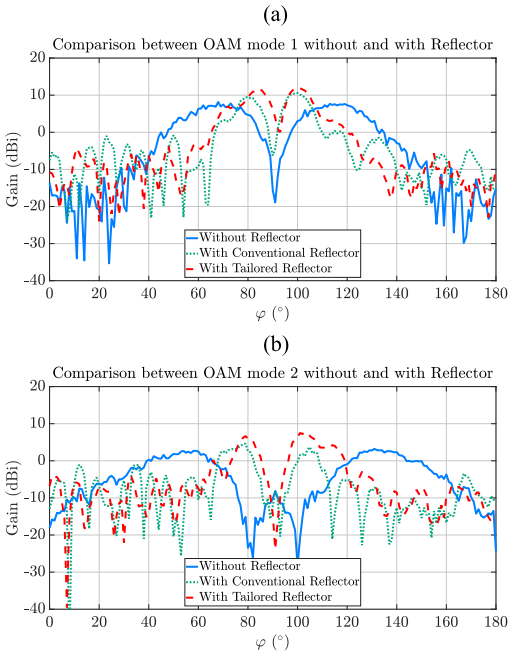

FIGURE 23. The measured gain (dBi) comparison between UCA without reflector, with conventional reflector, and with tailored reflector with rectangular ground plane shape 60 mm × 60 mm (height of 90 mm and angle of 45°) at $\varphi = 0°$ (*H*-plane) for the OAM mode order 1 (a), and 2 (b).

VIII. CONCLUSION

In this article, a novel lens and reflector are designed for OAM waves in order to overcome the large beam divergence inherent to OAM waves which are generated by uniform circular patch array (UCA) at 10 GHz. Both the tailored lens and the tailored reflector are compared to the conventional ones demonstrating better simulated and measured gain. Particularly, the tailored lens with a height r_0 of 93 mm has a simulated gain enhancement of 5.8 dB and 4.8 dB of measured gain for the first OAM mode order compared to the gain of a UCA without lens. Concerning the conventional lens, it provides a 1.8 dB simulated gain enhancement and 1.7 dB measured one. Furthermore, the improved gain of the tailored reflector reveals that it is more effective than the conventional one until it reaches a height r_0 of 1.5λ and an angle ϑ of 38°, separately. A tailored reflector fed by a UCA on rectangular ground plane (60 mm × 60 mm) with a height r_0 of 90 mm and an angle ϑ of 45° has a simulated gain improvement of 8.3 dBi and measured one of 3.9 dB for the first OAM mode order compared to the gain of a UCA without reflector. Whereas the conventional reflector has a 7 dB simulated gain enhancement and 2.5 dB measured one. Moreover, the tailored lens and reflector have a further advantage over the conventional ones through saving material consumption. This interest appears more obvious when higher OAM mode orders are applied with the aid of extra widely separated antennas. As a summary, this study demonstrates that the vortex waves need a tailored lens or a tailored reflector to decrease the beam divergence effectively as a function of all OAM mode orders which is necessarily needed for applications such as the target localization with vortex waves.

REFERENCES

[1] L. Allen, M. W. Beijersbergen, R. J. C. Spreeuw, and J. P. Woerdman, "Orbital angular momentum of light and the transformation of Laguerre–Gaussian laser modes," *Phys. Rev. A, Gen. Phys.*, vol. 45, no. 11, pp. 8185–8189, Jun. 1992.
[2] C. Zhang and L. Ma, "Millimetre wave with rotational orbital angular momentum," *Sci. Rep.*, vol. 6, no. 1, pp. 1–8, Sep. 2016.
[3] J. J. Chen, Q. N. Lu, F. F. Dong, J. J. Yang, and M. Huang, "Wireless OAM transmission system based on elliptical microstrip patch antenna," *Opt. Exp.*, vol. 24, no. 11, pp. 11531–11538, May 2016.
[4] M. Barbuto, M.-A. Miri, A. Alu, F. Bilotti, and A. Toscano, "A topological design tool for the synthesis of antenna radiation patterns," *IEEE Trans. Antennas Propag.*, vol. 68, no. 3, pp. 1851–1859, Mar. 2020.
[5] Q. Bai, A. Tennant, B. Allen, and M. U. Rehman, "Generation of orbital angular momentum (OAM) radio beams with phased patch array," in *Proc. Loughborough Antennas Propag. Conf. (LAPC)*. Loughborough, U.K.: IEEE, Nov. 2013, pp. 410–413.
[6] P. Schemmel, G. Pisano, and B. Maffei, "Modular spiral phase plate design for orbital angular momentum generation at millimetre wavelengths," *Opt. Exp.*, vol. 22, no. 12, pp. 14712–14726, Jun. 2014.
[7] F. E. Mahmouli and S. D. Walker, "4-Gbps uncompressed video transmission over a 60-GHz orbital angular momentum wireless channel," *IEEE Wireless Commun. Lett.*, vol. 2, no. 2, pp. 223–226, Apr. 2013.
[8] F. Qin, L. Wan, L. Li, H. Zhang, G. Wei, and S. Gao, "A transmission metasurface for generating OAM beams," *IEEE Antennas Wireless Propag. Lett.*, vol. 17, no. 10, pp. 1793–1796, Oct. 2018.
[9] T. Nguyen, R. Zenkyu, M. Hirabe, T. Maru, and E. Sasaki, "A study of orbital angular momentum generated by parabolic reflector with circular array feed," in *Proc. Int. Symp. Antennas Propag. (ISAP)*. Okinawa, Japan: IEEE, 2016, pp. 708–709.
[10] W. Zhang, S. Zheng, X. Hui, R. Dong, X. Jin, H. Chi, and X. Zhang, "Mode division multiplexing communication using microwave orbital angular momentum: An experimental study," *IEEE Trans. Wireless Commun.*, vol. 16, no. 2, pp. 1308–1318, Feb. 2017.
[11] M. H. Hassan, A. A. Abbas, A. Jimenez-Saez, A. M. Ahmad, B. Sievert, M. Schussler, A. Rennings, K. Solbach, T. Kaiser, R. Jakoby, A. Sezgin, and D. Erni, "Passive orbital angular momentum RFID tag based on dielectric resonator arrays," in *Proc. 3rd Int. Workshop Mobile THz Syst. (IWMTS)*, Essen, Germany, Jul. 2020, pp. 1–4.
[12] M. H. Hassan, B. Sievert, J. T. Svejda, A. A. Abbas, A. Jimenez-Saez, A. M. Ahmad, M. Schubler, A. Rennings, K. Solbach, T. Kaiser, R. Jakoby, A. Sezgin, and D. Erni, "OAM mode order conversion and clutter rejection with OAM-coded RFID tags," *IEEE Access*, vol. 8, pp. 218729–218738, 2020.
[13] K. Liu, X. Li, Y. Gao, H. Wang, and Y. Cheng, "Microwave imaging of spinning object using orbital angular momentum," *J. Appl. Phys.*, vol. 122, no. 12, Sep. 2017, Art. no. 124903.
[14] M. J. Padgett, F. M. Miatto, M. P. J. Lavery, A. Zeilinger, and R. W. Boyd, "Divergence of an orbital-angular-momentum-carrying beam upon propagation," *New J. Phys.*, vol. 17, no. 2, Feb. 2015, Art. no. 023011.
[15] X. Bai, Y. Sun, P. Hu, J. Chen, W. Yan, X. Liang, C. He, J. Geng, and R. Jin, "Improvement on the multi-mode beams divergence of oam array by using Fabry–Perot cavity," in *Proc. IEEE Int. Symp. Antennas Propag. USNC/URSI Nat. Radio Sci. Meeting*. San Diego, CA, USA: IEEE, Jul. 2017, pp. 2193–2194.
[16] H. Fukumoto, H. Sasaki, D. Lee, and T. Nakagawa, "Beam divergence reduction using dielectric lens for orbital angular momentum wireless communications," in *Proc. Int. Symp. Antennas Propag. (ISAP)*. Okinawa, Japan: IEEE, Oct. 2016, pp. 680–681.
[17] Y. Yao, X. Liang, W. Zhu, J. Li, J. Geng, R. Jin, and K. Zhuang, "Realizing orbital angular momentum (OAM) beam with small divergence angle by luneberg lens," in *Proc. IEEE Int. Symp. Antennas Propag. USNC/URSI Nat. Radio Sci. Meeting*. San Diego, CA, USA: IEEE, Jul. 2017, pp. 367–368.
[18] Y. Yao, X. Liang, W. Zhu, J. Geng, and R. Jin, "Synthesizing orbital angular momentum beam with small divergence angle," in *Proc. 6th Asia–Pacific Conf. Antennas Propag. (APCAP)*, Xi'an, China: IEEE, Oct. 2017, pp. 1–3.
[19] Z. Shi, Y. Jianjia, X. Cao, R. Feng, H. Zhang, and S. N. Burokur, "Omnidirectional radiation lens design of vortex beam carrying orbital angular momentum based on spatial transformation," in *Proc. 13th Eur. Conf. Antennas Propag. (EuCAP)*. Krakow, Poland: IEEE, 2019, pp. 1–4.

[20] M. H. Hassan, M. Al-Mulla, B. Sievert, A. Rennings, and D. Erni, "Evaluation of different phased array approaches for orbital angular momentum beam steering," in *Proc. German Microw. Conf. (GeMiC)*. Cottbus, Germany: IEEE, 2020, pp. 44–47.
[21] J. Y. Hong, W. Lee, B.-S. Kim, M.-S. Kang, J.-B. Kim, W. J. Byun, and M. S. Song, "Use of tractroid factor in deformed parabolic reflector antenna which transfers orbital angular momentum modes," in *Proc. Int. Conf. Inf. Commun. Technol. Converg. (ICTC)*, 2017, pp. 1229–1231.
[22] W. Byun, Y. Lee, B. S. Kim, K. S. Kim, M. S. Kang, and Y. H. Cho, "Simple generation of orbital angular momentum modes with azimuthally deformed Cassegrain subreflector," *Electron. Lett.*, vol. 51, no. 19, pp. 1480–1482, Sep. 2015.
[23] W. J. Byun and Y. H. Cho, "Generation of an orbital angular momentum mode based on a Cassegrain reflectarray antenna," in *Proc. IEEE Int. Symp. Antennas Propag. USNC/URSI Nat. Radio Sci. Meeting*, Jul. 2017, pp. 1191–1192.
[24] F. Qin, J. Yi, W. Cheng, Y. Liu, H. Zhang, and S. Gao, "A high-gain shared-aperture dual-band OAM antenna with parabolic reflector," in *Proc. 12th Eur. Conf. Antennas Propag. (EuCAP)*. London, U.K.: EuCAP, 2018, pp. 1–4, doi: 10.1049/cp.2018.0685.
[25] F. Qin, L. Li, Y. Liu, W. Cheng, and H. Zhang, "A four-mode OAM antenna array with equal divergence angle," *IEEE Antennas Wireless Propag. Lett.*, vol. 18, no. 9, pp. 1941–1945, Sep. 2019.
[26] M. H. Hassan, B. Sievert, A. Rennings, and D. Erni, "Reducing the divergence of vortex waves with a lens tailored to the utilized circular antenna array," in *Proc. 2nd Int. Workshop Mobile THz Syst. (IWMTS)*, Bad Neuenahr, Germany, Jul. 2019, pp. 1–4.
[27] K. Liu, Y. Gao, X. Li, and Y. Cheng, "Target scattering characteristics for OAM-based radar," *AIP Adv.*, vol. 8, no. 2, Feb. 2018, Art. no. 025002.
[28] A. Bisognin, N. Nachabe, C. Luxey, F. Gianesello, D. Gloria, J. R. Costa, C. A. Fernandes, Y. Alvarez, A. Arboleya-Arboleya, J. Laviada, F. Las-Heras, N. Dolatsha, B. Grave, M. Sawaby, and A. Arbabian, "Ball grid array module with integrated shaped lens for 5G backhaul/fronthaul communications in F-band," *IEEE Trans. Antennas Propag.*, vol. 65, no. 12, pp. 6380–6394, Dec. 2017.
[29] J. Thornton and K.-C. Huang, *Modern Lens Antennas for Communications Engineering*, vol. 39. Hoboken, NJ, USA: Wiley, 2013.
[30] C. A. Balanis, *Antenna Theory: Analysis and Design*. Hoboken, NJ, USA: Wiley, 2016.
[31] L. Weisgerber and A. E. Popugaev, "Multibeam antenna array for RFID applications," in *Proc. Eur. Microw. Conf.*, 2013, pp. 84–87.

MOHAMED HAJ HASSAN was born in Beirut, Lebanon. He received the B.Sc. degree in electrical engineering and the M.Sc. degree in high-frequency technology from the Technical University of Berlin, Berlin, Germany, in 2010 and 2012, respectively. He has worked as an RF Specialist in the industry for about two years. From 2015 to 2017, he was with the Technical University of Ilmenau, Ilmenau, Germany, in the field of ground penetration radar (GPR). Since 2017, he has a member with the Laboratory of General and Theoretical Electrical Engineering, University of Duisburg-Essen. His research interests include RF and antenna technology, mm-waves, vortex waves, electromagnetic metamaterials, and computational electromagnetics.

BENEDIKT SIEVERT (Member, IEEE) was born in Krefeld, Germany. He received the B.Sc. and M.Sc. degrees in electrical engineering/high-frequency systems from the University of Duisburg-Essen, in 2017 and 2019, respectively. Since 2017, he has been a member with the Laboratory of General and Theoretical Electrical Engineering, University of Duisburg-Essen. His research interests include mm-wave on-chip antennas, electromagnetic metamaterials, and theoretical and computational electromagnetics.

JAN TARO SVEJDA (Member, IEEE) received the B.Sc. degree in electrical engineering from the University of Applied Science, Düsseldorf, Germany, in 2008, and the M.Sc. and Dr.Ing. degrees in electrical engineering and information technology from the University of Duisburg-Essen, Duisburg, Germany, in 2013 and 2019, respectively, for his research work in the field of X-nuclei based magnetic resonance imaging. He is currently working as a Research Assistant with the Department of General and Theoretical Electrical Engineering, University of Duisburg-Essen, where he is involved in teaching several lectures and courses mainly in the field of electrical engineering. His general research interests include the all aspects of theoretical and applied electromagnetics, currently focusing on medical applications, electromagnetic metamaterials, and scientific computing methods.

AYA MOSTAFA AHMED received the B.Sc. and M.Sc. degrees in electrical engineering from German University, Cairo, Egypt, in 2011 and 2014, respectively. She is currently pursuing the Ph.D. degree with the Institute of Digital Communication Systems, Ruhr-Universität Bochum, Germany. Her research interests include MIMO radar signal processing, waveform design optimization, cognitive radars, direction of arrival (DOA) algorithms, and machine learning applications for radar resources management.

JAN BAROWSKI (Senior Member, IEEE) was born in Bochum, Germany, in 1988. He received the B.Sc., M.Sc., and Dr.Ing. degrees in electrical engineering from Ruhr-University Bochum, Bochum, in 2010, 2012, and 2017, respectively. Since 2012, he has been with the Institute of Microwave Systems, headed by Ilona Rolfes, Ruhr-University Bochum, as a Research Assistant. He is currently working as a Postdoctoral Research Scientist with the Institute of Microwave Systems, Ruhr-University Bochum. His research interests include radar signal processing, radar imaging, and material characterization techniques.

ANDREAS RENNINGS (Member, IEEE) received the Dipl.Ing. and Dr.Ing. degrees from the University of Duisburg-Essen, Germany, in 2000 and 2008, respectively. He studied electrical engineering at the University of Duisburg-Essen. He carried out his diploma work during a stay at the University of California at Los Angeles. From 2006 to 2008, he was with IMST GmbH, Kamp-Lintfort, Germany, where he has worked as an RF Engineer. Since then, he has been the Senior Scientist and a Principal Investigator with the Laboratory for General and Theoretical Electrical Engineering, University of Duisburg-Essen. His general research interests include all aspects of theoretical and applied electromagnetics, currently with a focus on medical applications and on-chip millimeter-wave/THz antennas. He received several awards, including the Student Paper Price at the 2005 IEEE Antennas and Propagation Society International Symposium and the VDE-Promotionspreis 2009 for the dissertation.

ILONA ROLFES (Member, IEEE) received the Dipl.Ing. and Dr.Ing. degrees in electrical engineering from Ruhr University Bochum, Bochum, Germany, in 1997 and 2002, respectively. From 1997 to 2005, she was with the High Frequency Measurements Research Group, Ruhr University Bochum, as a Research Assistant. From 2005 to 2009, she was a Junior Professor with the Department of Electrical Engineering, Leibniz University Hannover, Hannover, Germany, where she became the Head of the Institute of Radio frequency and Microwave Engineering in 2006. Since 2010, she has been leading the Institute of Microwave Systems, Ruhr University Bochum. Her research interests include high-frequency measurement methods for vector network analysis, material characterization, noise characterization of microwave devices, sensor principles for radar systems, and wireless solutions for communication systems.

AYDIN SEZGIN (Senior Member, IEEE) received the M.S. degree in communications engineering from Technische Fachhochschule Berlin (TFH), Berlin, in 2000, and the Ph.D. degree in electrical engineering from TU Berlin, in 2005. From 2001 to 2006, he was with the Heinrich-Hertz-Institut, Berlin. From 2006 to 2008, he held a postdoctoral position, and was also a Lecturer with the Information Systems Laboratory, Department of Electrical Engineering, Stanford University, Stanford, CA, USA. From 2008 to 2009, he held a postdoctoral position with the Department of Electrical Engineering and Computer Science, University of California at Irvine, Irvine, CA, USA. From 2009 to 2011, he was the Head of the Emmy-Noether Research Group on Wireless Networks, Ulm University. In 2011, he joined TU Darmstadt, Germany, as a Professor. He is currently a Professor of information systems and sciences with the Department of Electrical Engineering and Information Technology, Ruhr-Universität Bochum, Germany. His research interests include signal processing, communication, and information theory, with a focus on wireless networks. He has published several book chapters more than 40 journals and 140 conference papers in these topics. He has coauthored a book on multiway communications. He is a winner of the ITG-Sponsorship Award, in 2006. He was a first recipient of the prestigious Emmy-Noether Grant by the German Research Foundation in communication engineering, in 2009. He has coauthored papers that received the Best Poster Award at the IEEE Communication Theory Workshop in 2011, the Best Paper Award at ICCSPA in 2015, and the Best Paper Award at ICC in 2019. He has served as an Associate Editor for the IEEE TRANSACTIONS ON WIRELESS COMMUNICATIONS from 2009 to 2014.

DANIEL ERNI (Member, IEEE) received the Diploma degree in electrical engineering from the University of Applied Sciences Rapperswil (HSR), in 1986, the Diploma degree in electrical engineering from ETH Zürich, in 1990, and the Ph.D. degree in laser physics from the Laboratory for Electromagnetic Fields and Microwave Electronics, ETH Zürich, in 1996. Since 1990, he has been working with the Laboratory for Electromagnetic Fields and Microwave Electronics, ETH Zürich. From 1995 to 2006, he was the Founder and the Head of the Communication Photonics Group, ETH Zürich. Since October 2006, he has been a Full Professor of general and theoretical electrical engineering with the University of Duisburg-Essen, Germany. His current research interests include optical interconnects, nanophotonics, plasmonics, advanced solar cell concepts, optical and electromagnetic metamaterials, RF, mm-wave and THz engineering, biomedical engineering, bioelectromagnetics, marine electromagnetics, computational electromagnetics, multiscale and multiphysics modeling, numerical structural optimization, and science and technology studies (STS). He is a member of the Center for Nanointegration Duisburg-Essen (CeNIDE). He is the Co-Founder of the spin-off company airCode on flexible printed RFID technology. He is a Fellow of the Electromagnetics Academy and a member of the Swiss Physical Society (SPS), the German Physical Society (DPG), and the Optical Society of America (OSA).